

Ionization of sodium and lithium Rydberg atoms by 10-MHz to 15-GHz electric fields

C. R. Mahon,* J. L. Dexter,[†] P. Pillet,* and T. F. Gallagher
Department of Physics, University of Virginia, Charlottesville, Virginia 22901
 (Received 18 March 1991)

We have studied the ionization of Na ns and nd Rydberg atoms by $\sim 1\text{-}\mu\text{s}$ pulses of 10-MHz, 670-MHz, 2-GHz, and 4-GHz fields, bridging the gap between the previous measurements of ionization by $\sim 1\text{-}\mu\text{s}$ rise-time pulses and 8- and 15-GHz microwave fields. We have also studied the ionization of Li ns and nd Rydberg atoms by 4-, 8-, and 15-GHz fields, which, due to the smaller Li quantum defects, represents the high-frequency limit of nonhydrogenic microwave ionization. The Na measurements show that ionization at 10 MHz occurs without change in n at fields of $1/16n^4$ and $1/9n^4$. At 670 MHz $|m|=0, 1$, and 2 states are all ionized at fields between $1/3n^5$ and $1/9n^4$, indicating that transitions to higher- n states are occurring. As the frequency is raised further, to 2 and 4 GHz, the $|m|=0$ and 1 states exhibit an increasingly sharp threshold for ionization at $E=1/3n^5$, but the $|m|=2$ states are unlikely to ionize at this field, with ionization occurring mostly at higher fields, $1/3n^5 < E < 1/9n^4$, approaching the 15-GHz behavior of ionization at $E=1/9n^4$. At 4 GHz, Li $n=20$ $|m|=0$ and 1 states ionize at $E=1/3n^5$, but at $n \simeq 45$, $|m|=1$ states ionize at $E=1/9n^4$, and the $|m|=0$ states ionize at $E > 1/3n^5$. The $|m|=2$ states appear to ionize at $E=1/9n^4$. As the frequency is raised to 8 and then to 15 GHz, the transition of $|m|=0$ and 1 states to ionization at $E=1/9n^4$ occurs at lower n . When a small static field is applied, the Li ionization threshold fields drop from $1/9n^4$ to fields somewhat above $1/3n^5$. Together the Na and Li measurements show that microwave ionization depends on a rate-limiting step, which is a resonant multiphoton transition.

I. INTRODUCTION

Nonhydrogenic atoms exhibit very different behavior when exposed to microwave, as opposed to static or quasistatic, electric fields. In a static field an alkali-metal atom ionizes if its energy lies above the classical limit for ionization, that is, above the saddle point in the combined Coulomb Stark potential. Explicitly, ionization occurs if

$$E = W^2/4 \quad (1)$$

where E is the electric field and W is the energy of the state in question, both in a.u., which we shall use unless otherwise stated. Expressing Eq. (1) in terms of the principal quantum number n and ignoring Stark shifts yields the familiar expression for the field required for ionization, the classical field-ionization limit,

$$E = 1/16n^4. \quad (2)$$

In a static field an alkali-metal atom in the region labeled II in Fig. 1 lies above the classical field-ionization limit and will ionize. The ionization is via the coupling to the degenerate Stark continuum due to the finite-sized ionic core [1]. The process is really a form of autoionization, or more precisely, forced autoionization [2], and how rapidly it occurs depends upon the strength of the coupling.

Closely related to static field ionization is pulsed field ionization, which is widely used as a selective detection technique for Rydberg atoms. The only difference is that we must also consider how the atoms pass from zero field to the high ionizing field. In an electric field, the azimuthal angular momentum quantum number m is a good quantum number. As shown by the energy-level diagram of Fig. 1, which is a very rough representation of the Na $|m|=2$ states, the nearly degenerate zero-field l states of the same n are split by the Stark effect, and for $|m| \ll n$, the manifold of Stark states of principal quantum number n intersects the states of principal quantum number $n+1$ at field $E \simeq 1/3n^5$. The states of n and $n+1$ do not cross, as they do in H, but have avoided crossings of magnitude ω_0 due to the finite-sized ionic core [3]. These avoided crossings have the same origin as the coupling to the underlying Stark continuum responsible for ionization in static fields. Both couplings are approximately proportional to the quantum defects of the lowest l states of the m states under study. As a rough approximation the average avoided crossing size is given by $\omega_0 \simeq \delta_m/n^4$ where δ_m is the quantum defect of the $l=|m|$ states. Thus the couplings become weaker as $|m|$ increases.

If an atom initially in the nd state is exposed to a field which rises slowly, it follows an adiabatic path to the high ionizing field and ionizes at point A in Fig. 1 [4]. On the other hand, if the atom is exposed to a rapidly rising pulse which passes through the avoided crossings diabatically, the same atom follows the diabatic path to the high ionizing field which terminates at point B [5]. Note that in both cases ionization occurs at the classical ionization limit, but the energy, and hence the field required, are different. In an adiabatic passage the energy remains near the zero-field energy, and the ionizing field is given to a reasonable approximation by $E=1/16n^4$. On the other hand, a diabatic passage leads to ionization at a much lower energy, and a higher field is required, which is easily shown to be $E=1/9n^4$ [6]. In Na, of the opti-

thel angular momentum quantum number m is a good quantum number. As shown by the energy-level diagram of Fig. 1, which is a very rough representation of the Na $|m|=2$ states, the nearly degenerate zero-field l states of the same n are split by the Stark effect, and for $|m| \ll n$, the manifold of Stark states of principal quantum number n intersects the states of principal quantum number $n+1$ at field $E \simeq 1/3n^5$. The states of n and $n+1$ do not cross, as they do in H, but have avoided crossings of magnitude ω_0 due to the finite-sized ionic core [3]. These avoided crossings have the same origin as the coupling to the underlying Stark continuum responsible for ionization in static fields. Both couplings are approximately proportional to the quantum defects of the lowest l states of the m states under study. As a rough approximation the average avoided crossing size is given by $\omega_0 \simeq \delta_m/n^4$ where δ_m is the quantum defect of the $l=|m|$ states. Thus the couplings become weaker as $|m|$ increases.

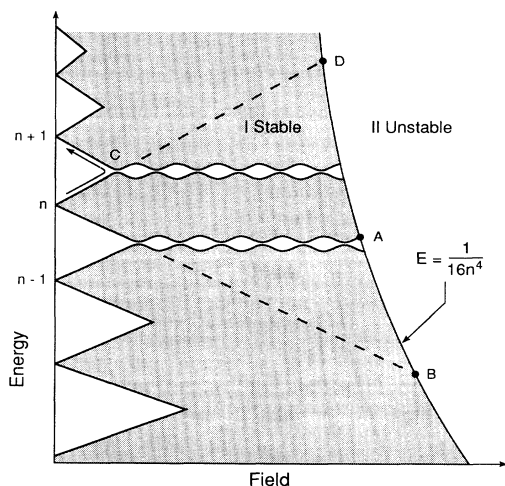


FIG. 1. Schematic drawing of the $n-1$, n , and $n+1$ Stark manifolds. Where the manifolds intersect the states have avoided crossings ω_0 . For ionizing fields with low slew rates the passage from low to high field is adiabatic and the red Stark state of n ionizes at the classical ionization limit at the field $1/16(n-1/2)^4$, point A. For ionizing fields with high slew rates the passage is diabatic and the red Stark state ionizes at the classical limit at the field $1/9n^4$, point B. The blue Stark state may ionize at the field $1/21n^4$ (point D) only by coupling to a rapidly ionizing red Stark state of high n . In a microwave field $E \geq 1/3n^5$ the atom ionizes via a sequence of Δn Landau-Zener transitions with the rate-limiting step being the $n \rightarrow n+1$ transition, point C.

cally accessible $|m| \leq 2$ states, the $|m|=0$ and 1 states have s and p states as their lowest l component, and hence the avoided crossings are large. The $|m|=2$ states have the d states as their lowest l component, and the avoided crossings are very small. Thus $|m|=2$ states are much more likely to exhibit diabatic passage. For Li, with even smaller quantum defects than Na, and therefore smaller avoided crossings, we expect more diabatic behavior than for sodium.

Ionization of sodium by a 15-GHz microwave field is very different from static field ionization [6,7]. The $|m|=0$ and 1 states ionize at a field of $E = 1/3n^5$, the field at which the n and $n+1$ Stark manifolds intersect and the lowest field at which there is an avoided level crossing between n and $n+1$ states. The threshold field for ionization of $E = 1/3n^5$ was first explained by Pillet *et al.* [6,7] using the following model, which we shall term the single-cycle Landau-Zener model. If atoms are initially excited to the nd and $|m|=0$ state, when the microwave field is turned on, the population becomes distributed over all the $|m|=0$ Stark states of the same n , with rapid transitions occurring between Stark states. Some of the atoms are always in the highest-energy Stark state. If the microwave field has an amplitude of $1/3n^5$ it brings the highest-energy Stark state of principal quantum number n to the avoided crossing with the lowest-energy Stark state of $n+1$, and a Landau-Zener transition can occur at the avoided crossing of the two states, as shown by point C of Fig. 1. On a single microwave cycle there is

an adequate n to $n+1$ transition probability if the angular frequency of the field, ω , is roughly comparable to the size of the avoided crossing, i.e., $\omega \sim \omega_0$, in which case the transition is neither purely adiabatic or diabatic. A similar description based on a single cycle of the field but several sets of interacting n and $n+1$ states was given by Mariani *et al.* to describe microwave ionization in He [8]. An adequate transition probability is $\sim 1\%$ since there are many microwave cycles in the $1\text{-}\mu\text{s}$ -long microwave pulse. Since the $n+1 \rightarrow n+2$ transition, and all higher Δn transitions, can occur at lower fields, the $n \rightarrow n+1$ transition is the rate-limiting step in a series of transitions to higher-lying states which culminates in ionization when it becomes classically allowed. As a result, it determines the microwave ionization threshold field. The $|m|=2$ states, on the other hand, ionize at a field of $E = 1/9n^4$. The $|m|=2$ states are composed of zero-field $l \geq 2$ states, all of which have small quantum defects, and, as a result, the avoided crossings between the Stark states of different n are very small compared to a microwave frequency of 15 GHz. Thus all level crossings are traversed diabatically, no Landau-Zener transitions to higher n occur, and ionization occurs as it does for a rapidly rising field pulse, at point B of Fig. 1. There are, however, rapid transitions between the $|m|=2$ Stark levels of the same n , allowing them all to ionize at the same field.

In a 15-GHz microwave field the Na $|m|=0$ and 1 states have avoided crossings of magnitude comparable to the microwave frequency, $\omega \sim \omega_0$, and the $|m|=2$ states have avoided crossings which are much smaller than the microwave frequency, $\omega \gg \omega_0$, which we shall call the high-frequency regime. This regime corresponds approximately to hydrogenic behavior. To date, no experiments have been done in the low-frequency regime, $\omega \ll \omega_0$, as a result there is no connection between the measurements of pulsed field ionization and ionization of Na by an 8-GHz microwave field [9], which is quite similar to ionization by a 15-GHz field. The only significant difference between the ionization of Na at 15 GHz is that at 8 GHz an $|m|=2$ ionization threshold is also observed at $E = 1/21n^4$, which corresponds to point D of Fig. 1 [9].

In an effort to observe the development from the low- to high-frequency regimes, i.e., from $\omega \ll \omega_0$ to $\omega \gg \omega_0$, we have measured the ionization of Na and Li atoms over a range of frequencies. As we have already noted, $\omega_0 \sim \delta_m/n^4$, so the different m states of Na and Li afford quite a range of values of ω_0 . Specifically, for Na $\delta_m = 1.35, 0.85$, and 0.015 for $|m|=0, 1$, and 2 ; and for Li $\delta_m = 0.30, 0.05$, and 0.0015 for $|m|=0, 1$, and 2 [10]. To reach the low-frequency regime, $\omega \ll \omega_0$, and bridge the gap between the pulsed field-ionization measurements and previous microwave ionization measurements we have measured the ionizing fields for Na in 10-MHz, 670-MHz, 2-GHz, and 4-GHz fields. To extend our measurements further into the high-frequency limit, $\omega \gg \omega_0$, we have reduced ω_0 by using Li, which has small quantum defects. We could also reduce ω_0 relative to ω by using higher frequencies or higher n states. Either of these approaches, however, raises ω relative to $1/n^3$, the ener-

gy spacing between n states, and in this case what we are here calling the high-frequency limit, $\omega \gg \omega_0$, no longer leads to ionization at $E = 1/9n^4$, but at lower fields instead [11].

As we shall see, the original single-cycle Landau-Zener description correctly identifies the critical field for the process, but applies too stringent a requirement to the ratio ω/ω_0 , i.e., $\omega \sim \omega_0$. The measurements reported here show that the coherent effect of many microwave cycles, leading to resonances, and the presence of many avoided crossings at $E > 1/3n^5$, both of which are absent from the single-cycle Landau-Zener model, are important. These notions are hardly surprising in light of the work of Stoneman, Thomson, and Gallagher [12], who made the connection between Landau-Zener transitions between Stark levels and multiphoton resonant transitions, and that of Christiansen-Dalgaard [13], who has developed a powerful Floquet approach to this problem, showing clearly that the observations are most generally understood in terms of multiphoton resonances.

Subsequent sections of the paper describe the experimental approach, the experimental observations, and discuss the evolution from low to high frequencies.

II. EXPERIMENTAL METHOD

The apparatus and experimental techniques are similar to those described previously [6,11]. For simplicity we first discuss the approach used at frequencies above 1 GHz. As shown in Fig. 2, a collimated beam of Na or Li atoms from a resistively heated source enters the microwave cavity where the atoms are excited by two tunable dye laser beams to a Rydberg state. The first laser is tuned to the $2s_{1/2} \rightarrow 2p_{1/2,3/2}$ transition for Li (671 nm), and the $3s_{1/2} \rightarrow 3p_{1/2,3/2}$ transition for Na (589 nm), while the second laser drives the transition $p_{1/2,3/2} \rightarrow \text{Rydberg } ns$ and nd states (410 nm for Na and 350 nm for Li). The atoms are then exposed to a microwave pulse of 1 μs duration, immediately after which a high voltage pulse is applied to a septum in the cavity.

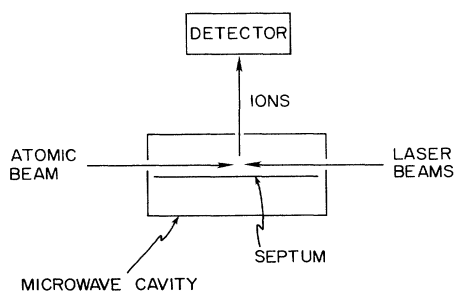


FIG. 2. Schematic diagram of the experimental arrangement. The counterpropagating atomic beam and laser beams enter through holes in a microwave cavity. In the cavity is a septum to which a voltage pulse is applied. The resulting field ionizes the atoms not ionized by the microwave field and forces the electrons (or ions) out of the cavity. The electrons (or ions) are then detected by a channel plate detector placed ≈ 2 cm above the cavity.

The pulsed field ionizes any remaining Rydberg atoms and drives out of the cavity and into a particle multiplier the electrons (or ions) produced by the field-ionization pulse. We do not detect the electrons (or ions) produced by the microwave field, rather those from the Rydberg atoms not ionized by the microwaves. The signal is recorded with a gated integrator as the microwave field in the cavity is varied.

The resonant cavities used at 2, 4, 8, and 15 GHz are all rectangular waveguide cavities operating on TE_{10n} modes, with n odd. The 8- and 15-GHz cavities are made of WR 90 and WR 75 copper waveguide with end flanges, and the 2- and 4-GHz cavities are machined from solid aluminum blocks. Choosing n odd places an antinode of the microwave electric field at the cavity center, as shown in Fig. 2. The microwave field is vertical, so the presence of the septum, a 0.7-mm-thick copper plate, does not affect the microwave electric field. The counterpropagating laser and atomic beams enter the cavities through 1.2-mm-diam holes in the cavity sidewalls and the ions are extracted through a 1.2-mm-diam hole in the center of the top of the cavity. This arrangement ensures that we only observe signals from atoms at the antinode of the microwave field. For reference the dimensions, mode, resonant frequency, and quality factor Q of each cavity are given in Table I.

The microwaves are generated by a Hewlett Packard (HP) 8616A oscillator or 8350B sweep oscillator with an 83540A or 83550A plug in. The oscillator output passes through 1- and 10-dB step attenuators, a microwave switch, and is then amplified to as much as 20 W by a Hughes traveling-wave tube amplifier (TWTA). The TWTA output is delivered to the microwave cavity via semirigid coaxial cable. In the line are a directional coupler, which allows power measurement with a HP 432 power meter, and a circulator, which both protects the TWTA from reflections and allows us to monitor the power reflected from the cavity.

Using the parameters of the cavities given in Table I we can relate the power incident on the cavity to the amplitude E of the electric field at the antinode of the cavity using the relation [6]

$$E = \left[\frac{4PQ}{\epsilon_0 V \pi f} \right]^{1/2}, \quad (3)$$

where P is the power input to the cavity in watts, V is the volume of the cavity in m^3 , Q is the quality factor, f is the resonant frequency, and ϵ_0 is the permittivity of free space, 8.854×10^{-12} F/m. Equation (3) gives the field in V/m. It is convenient to reexpress Eq. (3) in a form

TABLE I. Rectangular cavity parameters.

f (GHz)	Dimensions (cm^3)	Q	K ($\text{V/cm W}^{1/2}$)
15.22	$10.09 \times 1.90 \times 0.95$	850	217
7.89	$10.09 \times 2.28 \times 1.02$	1315	330
3.993	$5.30 \times 5.30 \times 1.27$	1530	402
1.988	$13.97 \times 8.89 \times 1.91$	457	120

which isolates the cavity parameters from the power and gives the field in V/cm. Explicitly

$$E = K\sqrt{P} \quad (4)$$

where the power conversion factor $K = (4Q/\epsilon_0 V \pi f)^{1/2} / (100 \text{ cm/m})$. In Eq. (4) K has the units of V/cm W^{1/2} and P is expressed in watts. In Table I we give the power conversion factors for the 2-, 4-, 8-, and 15-GHz cavities. Measurement of the attenuation between the directional coupler to the power meter and the cavity, and the fraction of the power coupled into the cavity allows us to relate the measured power to the field in the cavity. We estimate that we can measure the electric field in the cavities with an uncertainty of $\pm 10\%$.

The microwave cavity used at 670 MHz differs substantially from the rectangular cavities described above. It is a cylindrically symmetric reentrant coaxial cavity shown in cross section in Fig. 3. It is in essence two quarter wave pieces of coaxial line shorted at the ends of the cavity and open at the center. The cavity is constructed of brass with height $L = 17.29$ cm, outer radius $r_o = 5.08$ cm, inner radius $r_i = 4.06$ cm, and gap width $d = 1.49$ cm. The cavity can also be thought of as a resonant LC circuit in which the horizontal center section is a capacitor and the vertical sections are inductors in parallel with the capacitor. The cavity has a resonant frequency of 672 MHz and a Q of 230. The cavity is excited by an Epsco PG5KB pulsed oscillator with a 5233HB3 plug in, which produces 1- μ s pulses at powers of up to 10 W.

The counterpropagating laser and atomic beams enter the cavity through 1.2-mm-diam holes in opposite sides of the outer cylinder and pass above the septum in the

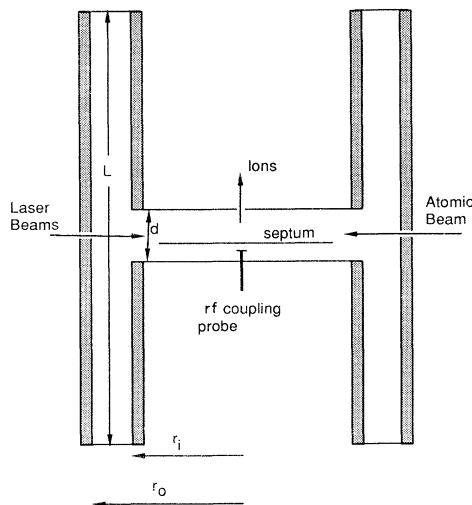


FIG. 3. Schematic of the reentrant cavity used at 670 MHz. Holes in the side of the outer conductor of the coaxial cylinders admit the counterpropagating laser and atomic beams. A voltage pulse applied to a septum in the gap pushes the ions out through a small hole in the top electrode of the inner conductor. The microwave power is coupled into the cavity by a probe positioned in the gap at the antinode of the electric field.

cavity gap. There is a 1.2-mm-diam hole in the center of the cavity, as shown, to allow the extraction of ions from the region of maximum electric field.

Equation (3) relates the energy stored in a rectangular cavity at the instant it is in the electric field to the input power to the cavity. We may apply the same method to the reentrant cavity once we develop an expression for the electric field distribution in the cavity. The potential difference between the inner and outer conductors of the coaxial cavity is given by [14]

$$V_o - V_i = V' \ln \left[\frac{r_o}{r_i} \right] \quad (5)$$

where V' is a constant. For a reentrant cavity this potential difference is the same as that between one of the inner conductors and the midpoint of the gap. Accordingly, the electric field at the gap midpoint is given by

$$E_0 = \frac{2}{d} V' \ln \left[\frac{r_o}{r_i} \right]. \quad (6)$$

For the electric field between the inner and outer conductors we assume a field distribution given by the field in the absence of the gap,

$$E(z, r) = \frac{V'}{r} \cos \left[\frac{\pi z}{L} \right]. \quad (7)$$

Using this field distribution we find a power conversion factor $K = 92.4 \text{ V/cm W}^{1/2}$. We estimate that we can measure the field at the interaction region, the center of the gap, with an uncertainty of $\pm 15\%$.

When radio-frequency (rf) fields are produced between metal plates any electrons present can be accelerated back and forth between the two plates, generating secondary electrons, resulting in a multipacting discharge [15]. The windows of rf field amplitudes for which the discharge is initiated scale as ω^2 and occur at ≈ 1000 –2000, 50–100, and $\ll 1$ V/cm for frequencies of 670, 100, and 10 MHz, respectively. The windows for 670 and 10 MHz are at sufficiently high and low fields, respectively, to allow us to produce fields of useful magnitudes for the present measurements. At 100 MHz, however, we were unable to pass through the multipacting window rapidly enough to avoid a discharge.

For the experiments done at 10 MHz we have used the electric field plate geometry shown in Fig. 4. The bottom plate is grounded, and the top plate is driven by a rf amplifier through an impedance matching π network. The grounded bottom plate is a square 7.6 cm on a side, and the septum and the top plate are squares 3.8 cm on a side, spaced by 0.61 cm. The septum is separated from the bottom plate by a 0.16-cm-thick sheet of Teflon. The π network and the plates constitute an LC circuit, which has a resonant frequency of 10 MHz and a Q of 100. The electrons are extracted through a 1.2-mm-diam hole in the center of the top plate.

The 10-MHz resonator is driven by a Wavetek 166 signal generator which is amplified to powers of up to 25 W by an ENI 325LA amplifier. At 10 MHz we no longer need to measure the power, but can directly measure the

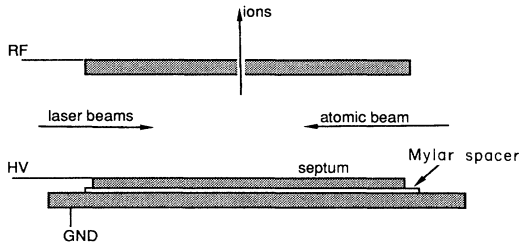


FIG. 4. 10- and 100-MHz cavity agreement. The rf is applied to the top plate, while the bottom plate is held at ground. The field-ionization pulse is applied to the septum, which is insulated from the bottom plate by a Mylar film. Ions are extracted through a hole in the center of the top plate for detection.

voltages on the plates with a fast high voltage probe. However, at this frequency the filling time of the cavity, the time for the field to attain 95% of its steady state value, is $\approx 20 \mu\text{s}$, a time far too long to allow us to turn the field on after the laser excitation. Instead, the experiment is conducted with the cavity continuously excited, and the data are acquired in a manner different from that used at the higher frequencies. Since the technique is peculiar to the 10-MHz experiments, we defer its description to the presentation of the 10-MHz observations.

III. OBSERVATIONS

Our approach in all the experiments at frequencies above 10 MHz has been to monitor the field-ionization signal from Rydberg atoms not ionized by the microwaves as a function of the attenuation of the power incident on the microwave cavity. In Fig. 5 we show typical data taken in this manner. Figure 5 is the field-ionization signal as a function of 4-GHz field amplitude when the Na $24d$ state is excited with the two lasers polarized both parallel and perpendicular to the field direc-

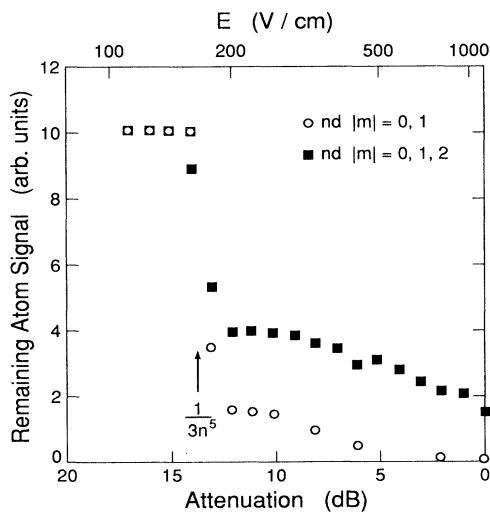


FIG. 5. Field-ionization signals for the Na $24d$ state as a function of the amplitude of the 4-GHz field. These data are obtained with $\mathbf{E}_{\text{laser}} \parallel \mathbf{E}_{\text{MW}}$ (solid circles) and $\mathbf{E}_{\text{laser}} \perp \mathbf{E}_{\text{MW}}$ (open squares). The arrow indicates the position of the field $1/3n^5$.

tion. For brevity we shall refer to these two choices of polarization as parallel and perpendicular. When we excite the nd states with parallel polarization we observe $|m|=0$ and 1 states, but with perpendicular polarization we observe $|m|=2$ states as well. Imperfections in the polarization and stray fields can destroy the purity of the selection rules, but the propensity remains. Excitation of the ns states necessarily results in $|m|=0$ states. In Fig. 5 there is a sharp decrease in the signal at the field $E = 1/3n^5$ indicating a sharp onset of ionization. We attribute this sharp threshold to the $|m|=0$ and 1 states. On the other hand, it is apparent that there is gradually increasing ionization beyond $E = 1/3n^5$, for both polarizations; however, it is a substantially larger fraction of the signal for perpendicular polarization, indicating that $|m|=2$ atoms are more likely to ionize at fields above $1/3n^5$.

A. Sodium

1. 4 GHz

With a 4-GHz microwave field we observe the ionization of the $|m|=0$ states alone when the ns states are excited. At the lowest- n states, $n \approx 18$, we observed a sharp transition from no ionization to 100% ionization over a $< 2\text{-dB}$ range of attenuation. At higher n , $n \approx 25$, the signals are very similar in appearance to the signal obtained with the lasers polarized parallel in Fig. 5, that is, they have a sharp onset of ionization and a tail at higher microwave fields. At $n = 30$ the tail at higher microwave field is more pronounced, and the initial decrease in the field-ionization signal, at $E \approx 1/3n^5$, is less sharp, $\sim 2 \text{ dB}$ wide. In Fig. 6 we plot the points at which the field-ionization signal has fallen by 50%, i.e., the field at which

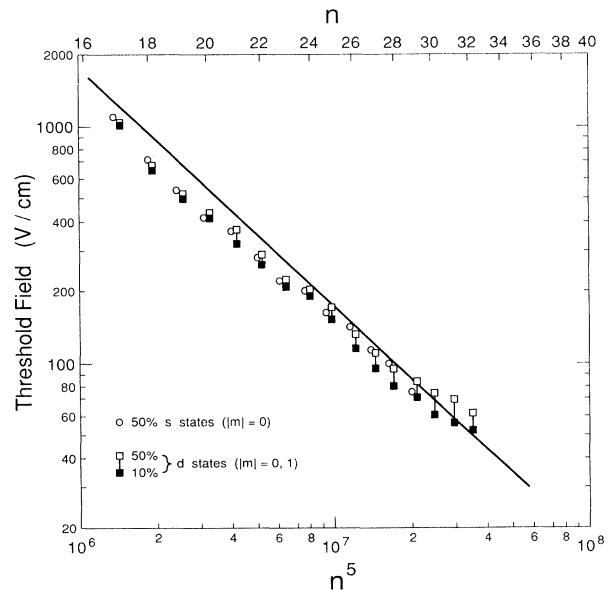


FIG. 6. Na 4-GHz thresholds. Shown also is the line corresponding to the field $1/3n^5$.

there is 50% ionization. In all the Na data, except for 10 MHz, we do not attempt to assign threshold fields to different $|m\rangle$ states. When the 50% ionization fields are plotted as a function of n they exhibit an $E \propto 1/n^5$ scaling as shown by Fig. 6. In Fig. 6 and all later plots of Na ionizing fields we plot the Na $(n+1)s$ state as having principal quantum number n to account for the quantum defect of 1.35. As shown by Fig. 6 the ns thresholds fall just below $E = 1/3n^5$, and, when fit to a $1/n^5$ dependence, they can be represented by

$$E_s = 1/3.43(30)n^5. \quad (8)$$

At $n \simeq 18$, with parallel polarization the nd states appear virtually identical to the s states of the same n , with all atoms being ionized at $E = 1/3n^5$. However, with perpendicular polarization, a substantial number of atoms are not ionized at this field. In fact we are not able to ionize these $|m|=2$ atoms, as we have insufficient microwave power. Figure 5 shows the behavior of the nd states at intermediate n . With parallel polarization a substantial fraction of atoms is not ionized at $E > 1/3n^5$, and this fraction is larger with perpendicular polarization. At $n \simeq 30$ with parallel polarization the initial decrease in the signal, while not as sharp as in Fig. 5, is readily observable. However, the high field tail is larger. The thresholds are also not as sharp as those of s states of the same n , indicating a difference between $|m|=0$ and 1 states. In contrast, at $n \simeq 30$ with perpendicular polarization there is hardly a noticeable distinction between the initial drop in the signal and the tail. In Fig. 6 we plot the 50% and the 10% ionization fields of the nd atoms excited with parallel polarization, or $|m|=0$ and 1 states. The fields exhibit a $1/n^5$ dependence, as shown by Fig. 6, and fitting the 50% ionization fields to this dependence gives

$$E_d = 1/3.25(45)n^5. \quad (9)$$

A feature of Fig. 6 worth noting is the fact that the high- n 50% points seem to fall above an $E \propto 1/n^5$ dependence. It is also apparent that the 50% ionization fields deviate more from a $1/3n^5$ dependence than the 10% fields for these n .

As shown by Fig. 5, and discussed in the preceding paragraph, when the nd states are excited there is a broad ionization feature extending from $E \simeq 1/3n^5$ to $E \simeq 1/9n^4$. This feature is more prominent with the lasers polarized perpendicular to the field direction than parallel to the field direction. Based on the polarization dependence of the observed signals it seems apparent that at 4 GHz the $m=2$ states begin to ionize when the field exceeds $1/3n^5$. However, at this field the transitions to high- n states are driven so inefficiently that the ionization rate increases more or less monotonically with the field amplitude, up to a field $\simeq 1/9n^4$.

2. 2 GHz

At a microwave frequency of 2 GHz the ns data are similar to the 4-GHz data, i.e., we observe a sharp onset of ionization at $E \simeq 1/3n^5$ and a tail extending to higher fields. However, the distinction between the onset and

the tail is not as clear as in the 4-GHz data of Fig. 5. As n is raised from 20 to 30 the tail becomes larger, and the distinction becomes increasingly less clear. In Fig. 7 we plot the fields at which there is 10% and 50% ionization. Fitting the 50% ionization fields to a $1/n^5$ dependence yields

$$E_s = 1/3.19(16)n^5. \quad (10)$$

Measurement of the threshold fields for the nd states reveals that they are nearly identical to the ns thresholds of the same n , irrespective of the laser polarization, although the field-ionization signal decreases a little less rapidly as a function of microwave field with perpendicular polarization than with parallel polarization, as shown by Fig. 8, for the 29d state.

In Fig. 7 we plot the 50% ionization fields for the nd states with parallel and perpendicular polarization. Also shown are the 10% fields for parallel polarization. As at 4 GHz, the fields generally follow an $E = 1/n^5$ dependence, the fields for high nd states are higher than $1/3n^5$, and the 50% ionization fields diverge substantially from the 10% ionization fields as n is increased. The measured nd 50% ionization fields obtained with parallel polarization can be fit to an $E \propto 1/n^5$ dependence, yielding

$$E_d = 1/2.98(30)n^5. \quad (11)$$

In sum there are two differences between 2 GHz and the higher frequencies. First, we are not able to see a striking difference between the $|m|=2$ ionization and the $|m|=0$ and 1 ionization. Second, the ionization can no longer be described as having a clear threshold field; it is clearly a process with a rate which varies smoothly with the microwave field amplitude.

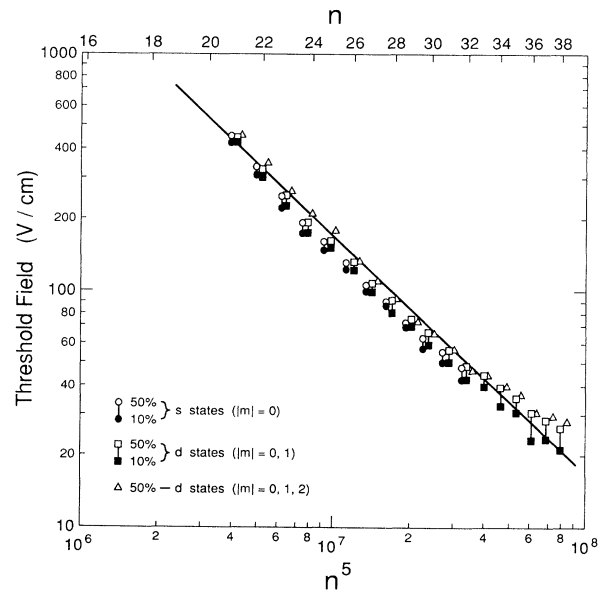


FIG. 7. Na 2-GHz thresholds. Included for reference is the line $1/3n^5$.

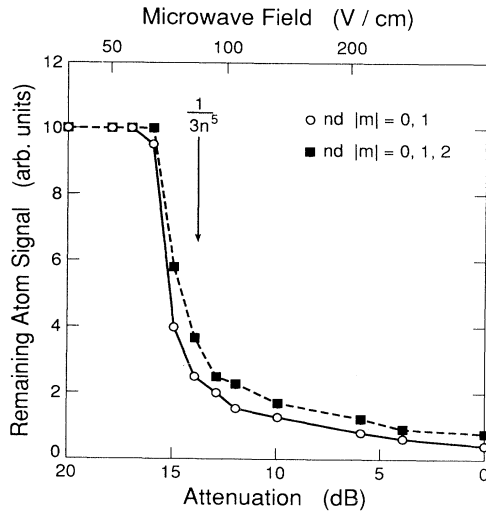


FIG. 8. Field-ionization signals for the Na 29d state as a function of 2-GHz field strength for both lasers polarized parallel to the microwaves, $\mathbf{E}_{\text{laser}} \parallel \mathbf{E}_{\text{MW}}$ (open circles), and perpendicular to the microwaves, $\mathbf{E}_{\text{laser}} \perp \mathbf{E}_{\text{MW}}$ (closed squares). Aside from the larger high field tail, with perpendicular polarization, there is negligible difference between the two polarizations. The arrow indicates the position of the field $1/3n^5$.

3. 670 MHz

With a frequency of 670 MHz the thresholds for the lowest ns states are qualitatively similar to the thresholds obtained at a frequency of 2 GHz; there is a sharp onset of ionization at $E = 1/3n^5$ and a gradual increase in the ionization as the field is raised. In the observed signal this behavior is manifested as a sharp decrease in the number of atoms in the field-ionization signal at $E \approx 1/3n^5$, with a tail extending to higher field. As n is increased the sharpness of the onset of ionization diminishes, and at high n it is difficult to discern two components in the signal.

The fields that produce 10% and 50% ionization are plotted in Fig. 9, from which it is apparent that these fields exhibit an $E \propto 1/n^5$ dependence. A fit to the observed 50% ionization fields shown in Fig. 9 yields

$$E_s = 1/2.39(15)n^5. \quad (12)$$

We note in Fig. 9 that the 10% and 50% fields differ considerably more than for 2 GHz. When the low- n , ≈ 22 , nd states are excited with parallel polarization the signals appear virtually identical to those of the ns states, but with perpendicular polarization the amplitude of the signal at high microwave fields is larger. As n is increased the thresholds observed with parallel polarization evolve in the same way as do the ns thresholds. With perpendicular polarization the field-ionization signal decreases more gradually with increasing microwave power, as shown by Fig. 10, the field-ionization signals for the 31d state. The 10% and 50% ionization fields are plotted in Fig. 9, which makes the $E \propto 1/n^5$ dependence quite evident. As shown by Fig. 9, the 10% ionization fields follow closely $1/3n^5$ as n is increased, but the 50% fields increase rather sharply, reaching fields as much as 50%

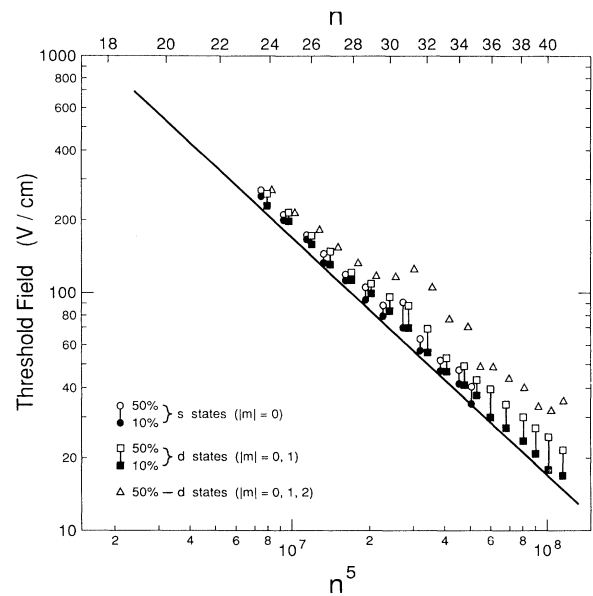


FIG. 9. Na 670-MHz thresholds. Included is the line $1/3n^5$.

higher than $1/3n^5$.

The 50% ionization fields obtained with parallel polarization may be fit to a $1/3n^5$ dependence, yielding

$$E_d = 1/2.24(19)n^5. \quad (13)$$

The onset of ionization occurs at $E \approx 1/3n^5$, the $E \propto 1/n^5$ scaling showing clearly that ionization occurs via a sequence of transitions through higher- n states.

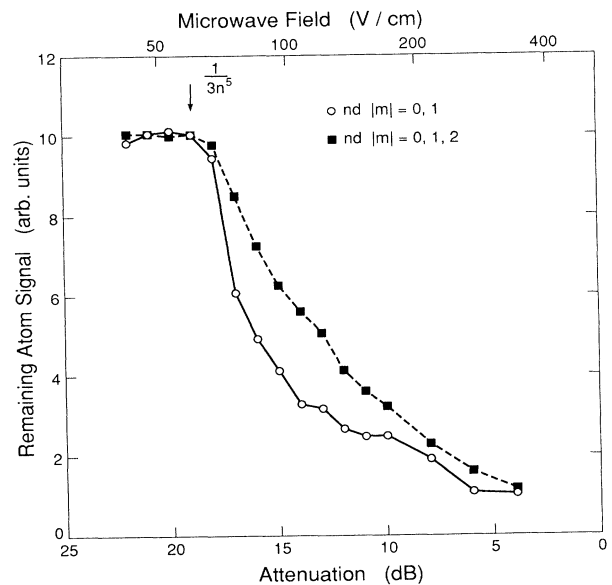


FIG. 10. Field-ionization signals for the Na 31d state as a function of 670-MHz field for $\mathbf{E}_{\text{laser}} \parallel \mathbf{E}_{\text{MW}}$ (open circles) and $\mathbf{E}_{\text{laser}} \perp \mathbf{E}_{\text{MW}}$ (closed squares). The ionization threshold is clearly sharper for parallel polarization, indicating that $|m|=2$ states require higher fields for ionization.

However, the probability of making the transition via the lowest field avoided crossing is not high enough that ionization exhibits a sharp threshold field. Rather, a field extending further into the region where many Stark manifold states have avoided crossings is required.

4. 10 MHz

Due to the long response time of the 10-MHz resonator, we have been forced to use a different experimental approach. We continuously excite the cavity and excite the atoms in zero-field Rydberg states by synchronizing the lasers to fire at a zero crossing of the rf field. The obvious way to measure the ionization fields is to attenuate the rf power, but attenuation of the rf power introduces phase shifts in the rf field, altering the synchronization, and thus the field when the laser fires. Since the laser pulse is 5 ns long, even in the best case the laser is exciting the atoms at $\pm 9^\circ$ from the zero crossing, at which point there can be a significant field. To minimize the fields when the atoms are excited, we have taken the data in a different way. We excite the atoms as described above, and after 1 μ s we apply a field-ionization pulse to detect any Rydberg atoms not ionized by the 10-MHz field. We monitor the field-ionization signal at a fixed rf field while the $3p \rightarrow$ Rydberg laser is scanned through the Rydberg series. This process is repeated for many 10-MHz field strengths to build up synthetic field-ionization signals analogous to those recorded directly at higher frequencies. A typical series of such scans is shown in Fig. 11 for 10-MHz fields of 0, 650, and 1325 V/cm. As can be seen in Fig. 11, the np states are still visible when the rf is on, due to the finite temporal width of the laser pulse, but the spectra are reasonably similar to the zero-field spectra. The electric field threshold for any state is then determined by measuring its strength in the excitation spectra at different rf field strengths. To account for any long-term drifts in the signal intensity we normalize to the strengths of the first two peaks of each scan, which are recorded in the absence of any rf field.

We can synthesize field-ionization signals from data such as those shown in Fig. 11, and as an illustration we show in Fig. 12 the $n = 34$ signals with parallel and perpendicular polarizations. In doing so we treat the $(n+1)s$, $(n+1)p$, and nd states collectively as a Rydberg state of principal quantum number n . The vertical arrows of Fig. 12 show the positions of the fields $1/16n^4$ and $1/9n^4$. With parallel polarization we observe a clear decrease of the signal to zero at $E = 1/6n^4$. We plot the fields at which there is 50% ionization in Fig. 13. As shown by Fig. 12, the excitation with perpendicular polarization leads to a signal out to much higher fields, which we interpret as arising from $|m|=2$ states. In some cases the $|m|=2$ signal disappears and reappears in the region $E > 1/3n^5$, and we assign the $|m|=2$ ionization field as the lowest field value at which we observe the field-ionization signal to disappear. The $|m|=2$ ionization fields are plotted in Fig. 13. Fitting these thresholds to $1/n^4$ field dependences gives

$$\begin{aligned} E &= 1/17.0(1.2)n^4(|m|=0,1), \\ E &= 1/8.96(94)n^4(|m|=2). \end{aligned} \quad (14)$$

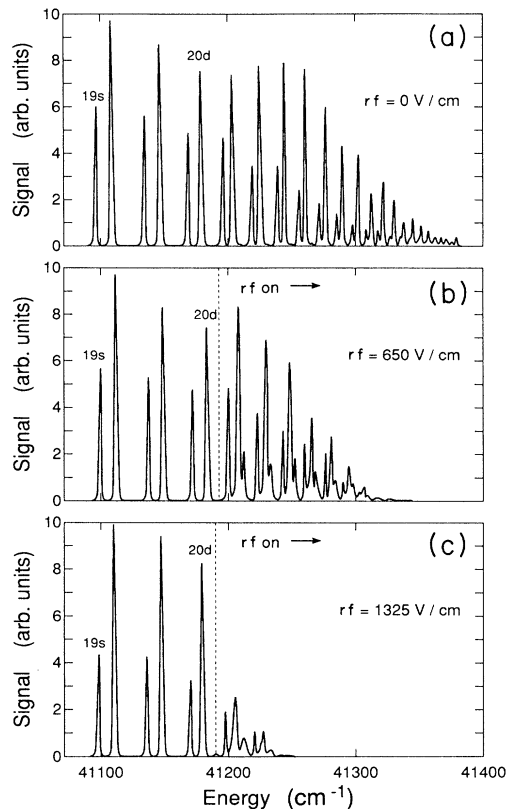


FIG. 11. Representative field-ionization signals obtained by scanning the second laser over the Rydberg series with different 10-MHz field amplitudes. The first two peaks of each scan are recorded in zero 10-MHz field for normalization purposes. The 10-MHz fields are (a) 0 V/cm, (b) 650 V/cm, and (c) 1325 V/cm.

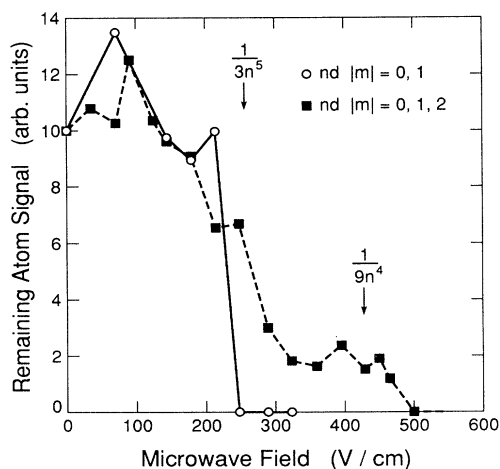


FIG. 12. Field-ionization signals for the $34d$ state synthesized from scans such as the ones in Fig. 11 in which the two lasers are polarized parallel (open circles) and perpendicular (closed squares) to the 10-MHz field. The fields $1/3n^5$ and $1/9n^4$ are indicated by arrows.

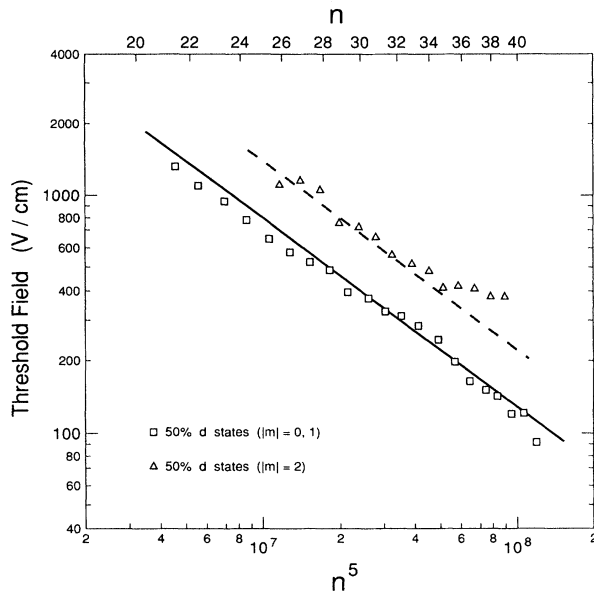


FIG. 13. Na 10-MHz thresholds including for reference the $1/16n^4$ and $1/9n^4$ field dependences.

As shown by Fig. 13, the fields follow the $1/16n^4$ and $1/9n^4$ dependences expected on the basis of previous field-ionization experiments [4,5]. Our present resolution is inherently worse, for two reasons. First, the attenuation steps are too large. Second, though synchronized to fire at a zero crossing of the rf field, the 5 ns width of the exciting laser ensures that a fraction of the atoms are excited in a nonzero field. As a result, several Stark states are populated, and their different ionization fields and the possibility of field reversal [16] obscure any fine details.

B. Lithium

1. 15 GHz

In a 15-GHz field the Li ns states exhibit a single ionization threshold, corresponding to $E = 1/3n^5$. For the lowest n states studied, $n \approx 20$, the thresholds are sharp, < 1 dB wide. For higher- n states the thresholds became gradually more broad, and for the highest n studied, $n = 32$, the thresholds are ≈ 10 dB wide. The fields at which there is 50% ionization, the threshold fields, are plotted in Fig. 14. Fitting these threshold fields to an n^{-5} dependence gives

$$E_s = 1/3.33(22)n^5. \quad (15)$$

When the nd states are excited with parallel polarization the thresholds show a much more complicated evolution as a function of n than do the Na data. In Fig. 15 we show 15-GHz field-ionization signals for $n = 24, 32, 36, 44$, and 54 d states. For the low nd states, such as $24d$ of Fig. 15, there is only a single, quite broad (6 dB), threshold observed at $E \approx 1/3n^5$. As we have only sufficient microwave power to generate a microwave field of up to 800 V/cm, for the $n = 24$ state we are only able to ionize up to 80% of the atoms. As a result it is impossible to be sure whether or not there is a high field tail to the ionization signal, although such appears to be the case.

As n is increased the threshold becomes increasingly broad. For $n = 32$, the threshold is ≈ 25 dB wide in the microwave power, extending from $E = 1/3n^5$ to $1/9n^4$. By comparing this $32d$ state, $|m|=0$ and 1, threshold to the corresponding $|m|=0$ threshold of the s state of the same n , we conclude that the broadening of the $32d$

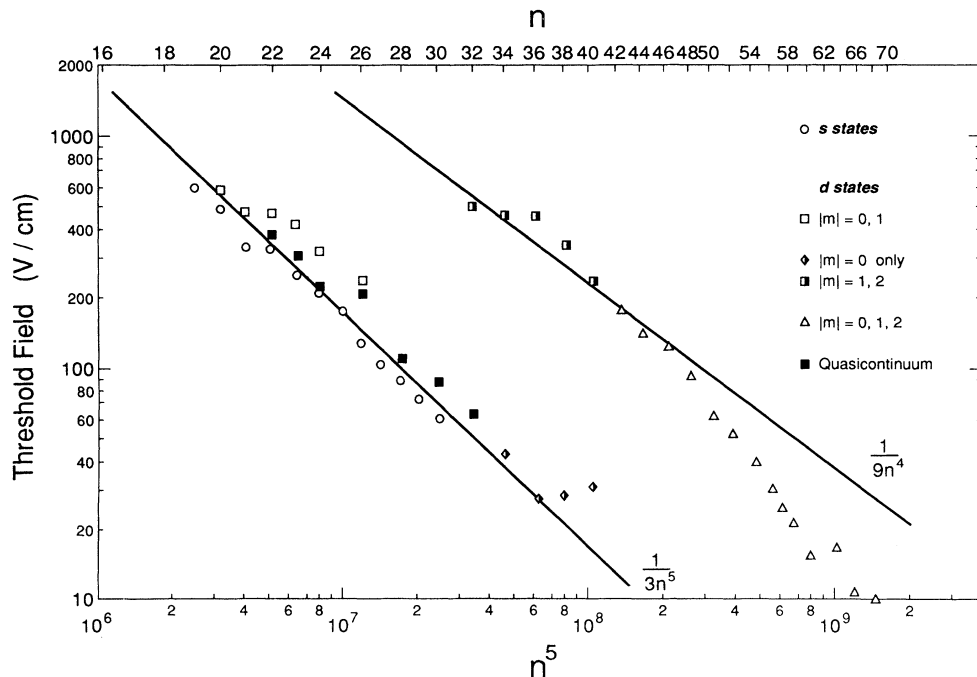


FIG. 14. Li 15-GHz threshold fields. Shown also for reference are the $1/3n^5$ and $1/9n^4$ field dependences.

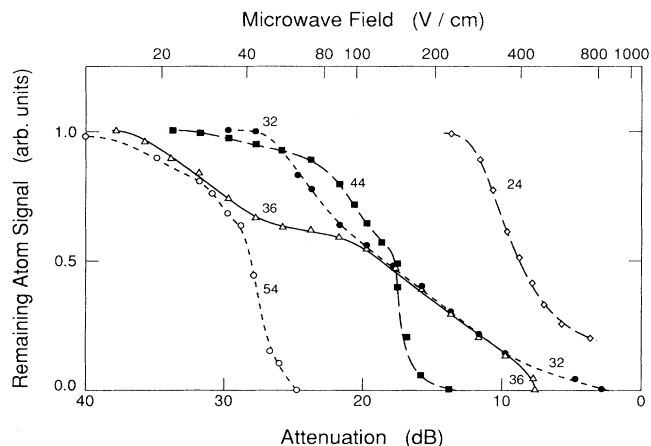


FIG. 15. Representative 15-GHz Li nd field-ionization signals with $E_{\text{laser}} \parallel E_{\text{MW}}$ for $n = 24, 32, 44, 36,$ and 54 .

threshold is due primarily to the $|m|=1$ states.

As n is further increased it becomes possible to see multiple thresholds. For example, in the $n=36$ scan of Fig. 15 there are two distinct decreases in the field-ionization signal, between 10 and 50 V/cm, and between 100 and 400 V/cm. We attribute the former to ionization of $|m|=0$ states at $E \approx 1/3n^5$ and the latter to ionization of $|m|=1$ states at $1/21n^4 < E < 1/9n^4$. For $n=36$, $1/3n^5 = 28$ V/cm and $1/9n^4 = 340$ V/cm. The fact that there is almost no $|m|=1$ ionization at $E \sim 1/3n^5$ allows us to discern the $|m|=0$ threshold.

For $n > 40$ there is no discernible threshold at $E \approx 1/3n^5$. We infer that the $E = 1/3n^5$ $|m|=0$, threshold develops into a broad threshold extending from $E = 1/3n^5$ to $1/9n^4$. For the highest n only the single sharp $E = 1/9n^4$ threshold is observed just as for the $|m|=1$ states of lower n . In Fig. 15 the $n=44$ and 54 states correspond to this latter case for which most, $> 85\%$, of the atoms ionize only in fields $E > 1/21n^4$, and $> 50\%$ ionize at $E = 1/9n^4$.

With perpendicular polarization, leading also to the excitation of the $|m|=2$ states as well, for all n we observed an increase in the number of atoms ionized at the field $E = 1/9n^4$. This observation indicates that the $|m|=2$ states do not ionize by Landau-Zener transitions at $E \sim 1/3n^5$ and that these states ionize by direct field ionization at the classical ionization field $E = 1/9n^4$.

From $|m|=0$ and 1 data such as those shown in Fig. 15 it is possible to extract $E = 1/3n^5$ threshold fields only for the lowest- n states, and $E = 1/9n^4$ threshold fields for the highest- n states. For intermediate n the variation of ionization with field is so gradual that it is of questionable utility to assign threshold fields and we have not done so. In Fig. 14 we plot the threshold fields observed at $E \approx 1/9n^4$. We simply note for now that for the highest $n > 48$ states the thresholds drop below $1/9n^4$ and begin to follow a $3/n^5$ field dependence. These high- n states have been referred to as the regime of chaotic motion [17–19], though the ionization process may be thought of in simpler terms [13], a discussion of which we defer to the following section. In assigning these threshold fields

we have used the midpoints of the final rapid decrease in the field-ionization signal, not the points at which there is 50% ionization. The latter values are meaningless in this case.

In spite of the fact that there is no apparent threshold at $E = 1/3n^5$ for the $32d$ state shown in Fig. 14, we can force the appearance of a threshold at $E \approx 1/3n^5$ by applying a small voltage to the septum, adding a small static field ~ 1 V/cm to the microwave field. This effect, first observed by Pillet, Mahon, and Gallagher [20], has been termed microwave ionization by quasicontinuum production. We defer until the next section a discussion of why this small field has such a dramatic effect; for now we simply note that the threshold fields so obtained are plotted in Fig. 14.

2. 8 GHz

The 8-GHz data do not differ dramatically from those obtained at 15 GHz. As we only had sufficient microwave power to ionize states of $n \geq 30$, and our laser linewidth allows resolution of s states of $n \leq 32$, our measurements at 8 GHz are therefore limited to the d states. Nevertheless, the development of the nd microwave ionization threshold at 8 GHz is also instructive, and representative examples of the nd data obtained with parallel polarization are shown in Fig. 16. The lowest $n=30d$ state shows a vestigial $E \approx 1/3n^5$ threshold, at $E \sim 80$ V/cm, as part of a slowly increasing ionization probability with increasing microwave field, covering the range $E = 1/3n^5 < E < 1/9n^4$. At $n=36$ it is impossible to discern a clear threshold at $E = 1/3n^5$, and as n is increased further the onset of ionization at $E \approx 1/3n^5$ becomes even less distinct. On the other hand, the sharp threshold at $E = 1/9n^4$ becomes more pronounced. As for 15 GHz we are able to force a $1/3n^5$ threshold by application of a small static field, again due to the quasicontinuum effect. With perpendicular polarization, we observe an increase in the amount of ionization which occurs at $E = 1/9n^4$, as expected. From these data we are only able to extract unambiguously the $E = 1/9n^4$ threshold fields, which are assigned in the same way as the 15-GHz data and are plotted in Fig. 17 along with the $\sim 1/3n^5$ quasicontinuum thresholds measured in small (~ 1 V/cm) static fields.

3. 4 GHz

With a microwave frequency of 4 GHz the results are qualitatively similar to those obtained at 8 and 15 GHz. For the s states a single $1/3n^5$ threshold is observed for $|m|=0$. For the lower n , $=18$ – 28 , the thresholds are sharp (2 dB). This point is made clearly by the $28s$ field-ionization signal shown in Fig. 18. For higher n there remains a sharp ≈ 2 dB drop in signal when the microwave field exceeds $1/3n^5$, though a high field tail begins to appear. For $n=32$ this tail is about 30% of the total s state signal. The large high field tail indicates that the microwave field is not driving the $n \rightarrow n+1$ transition efficiently at fields of $1/3n^5$; higher fields are required. The observed threshold fields are plotted in Fig. 19. Fitting these threshold fields to an n dependence gives

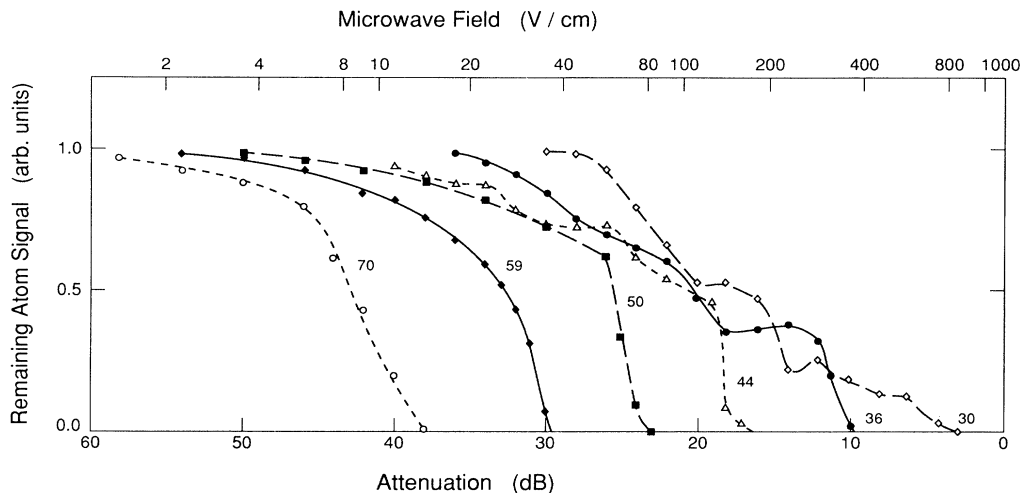


FIG. 16. Representative 8-GHz Li nd field-ionization signals with $E_{\text{laser}} \parallel E_{\text{MW}}$ for $n = 30, 36, 44, 50, 59,$ and 70 .

$$E_s = 1/3.61(35)n^5. \quad (16)$$

Also shown, for comparison, in Fig. 18 are the $28d$ signals obtained with parallel polarization in zero static field, and with a static field of 1 V/cm. In the absence of the static field the $28d$ ionization has a semblance of a threshold at $E = 1/3n^5$ but generally increases slowly as the microwave field is raised from $E = 1/3n^5$ to $1/9n^4$. However, with the static field due to the quasicontinuum formation by the small static field we see a clear threshold field at a field slightly in excess of the $28s$ threshold field.

In Fig. 20 we show representative data for a series of nd states obtained with parallel polarization. The lowest state, $n = 18$, exhibits a single, sharp, ≈ 2 -dB-wide, threshold at $E = 1/3n^5$. For higher n , $n = 26$, the thresh-

old broadens, extending from $1/3n^5$ to, presumably, $1/9n^4$. We interpret the broadening of the threshold to the $|m|=1$ states' ionizing over the field range $1/3n^5 < E < 1/9n^4$. For higher $n = 34$, two thresholds appear corresponding to $E = 1/3n^5$ and $1/9n^4$. We interpret the change in the signal from the $30d$ signal to the fact that the $|m|=1$ states do not ionize for $E < 1/9n^4$, allowing us to observe clearly the $|m|=0$ threshold at $E = 1/3n^5$. As n is further increased ionization begins to rise slowly at $E = 1/3n^5$, and there is a clear threshold at $E = 1/9n^4$. We attribute the slowly rising ionization to the $|m|=0$ states and the sharp threshold at $E = 1/9n^4$ to $|m|=1$ states. When perpendicular polarization is used to excite the nd states the most significant difference is that we are able to see the $E = 1/9n^4$ threshold more clearly at lower n due to the fact that the $|m|=2$ states

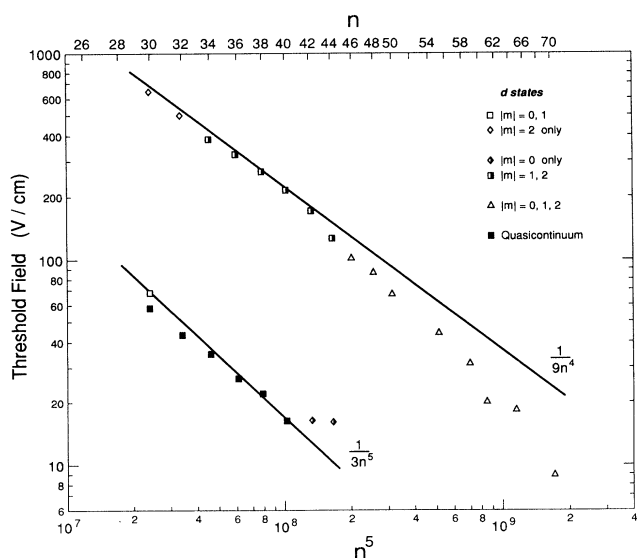


FIG. 17. Li 8-GHz threshold fields for the nd states. Shown also are the field dependences $1/3n^5$ and $1/9n^4$.

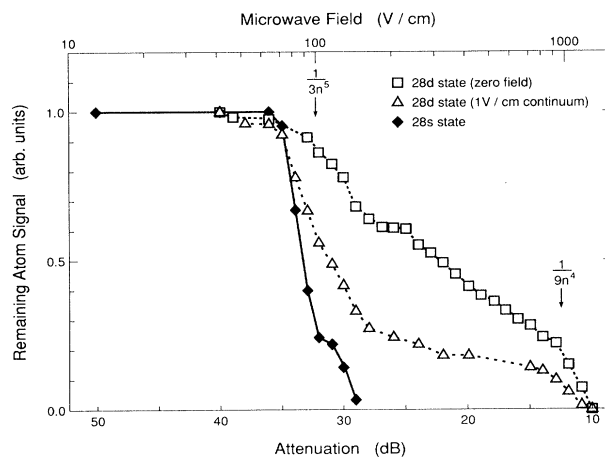


FIG. 18. Li field-ionization signals as a function of the 4-GHz microwave field for the $28s$ state (closed diamonds); and $28d$ state for $E_{\text{laser}} \parallel E_{\text{MW}}$ in zero static field (open squares), and in a ≈ 1 V/cm static field used to produce the quasicontinuum (open triangles). The $|m|=0$ threshold field is $1/3n^5$, and the high field $|m|=1$ threshold is $1/9n^4$. Producing the quasicontinuum allows the $|m|=1$ states to ionize at $E \approx 1/3n^5$.

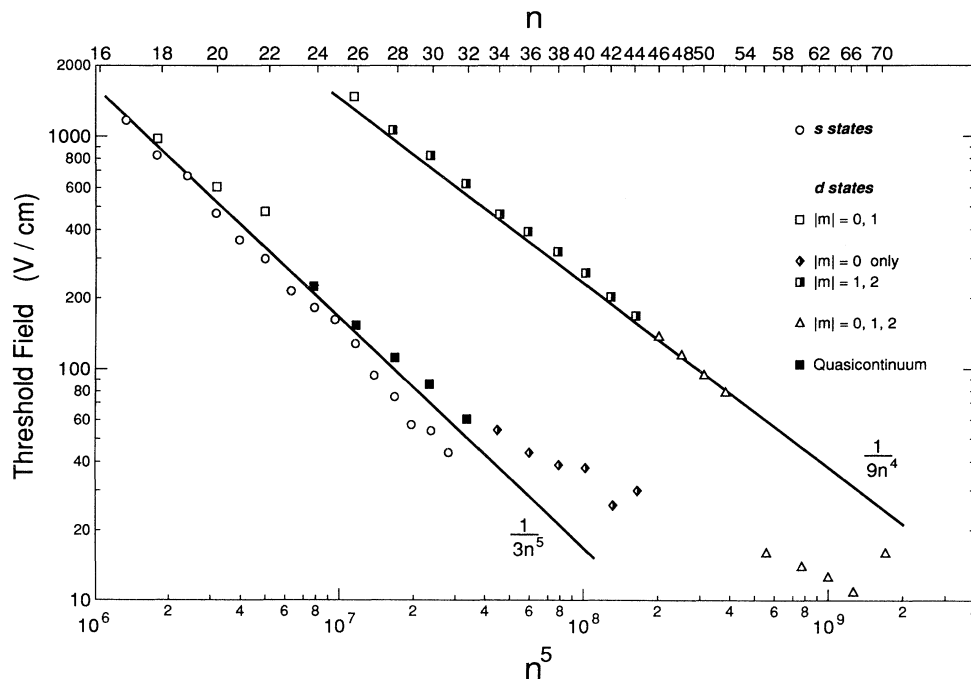


FIG. 19. Li 4-GHz threshold fields for ns states and nd states. Shown also are the field dependences $1/3n^5$ and $1/9n^4$.

only ionize at $E = 1/9n^4$ at 4 GHz.

As is the case at 8 and 15 GHz, there are clear threshold fields for the ns states, and for the nd states at fields $\sim 1/9n^4$. However, in most other cases the assignment of threshold fields is questionable at best, and we have not attempted to make such assignments. In Fig. 19, we plot the observed threshold fields, including $E \approx 1/3n^5$ threshold fields obtained by quasicontinuum production with a small static field.

IV. DISCUSSION

How alkali-metal atoms ionize as the frequency is increased from 10 MHz to 15 GHz is a question of the ex-

tent to which ionization occurs via transitions to higher- n states rather than by direct field ionization at $E = 1/9n^4$ or $1/16n^4$. In the initial microwave ionization measurements at 15 GHz ionization was found to occur at $E = 1/3n^5$, corresponding to the field required to drive the rate-limiting n to $n+1$ transition, and no resonance effects were observed. The rate-limiting transition was described as occurring via the extreme Stark states of the n and $n+1$ states, and a single-cycle Landau-Zener model was used to describe the transition. If $\omega \approx \omega_0$ this model predicts a threshold field of $E = 1/3n^5$, or, if the field is kept fixed at $E = 1/3n^5$, this model predicts a rather loose frequency requirement, $\omega \approx \omega_0$. The measurements described here show that, in fact, the rate-limiting transi-

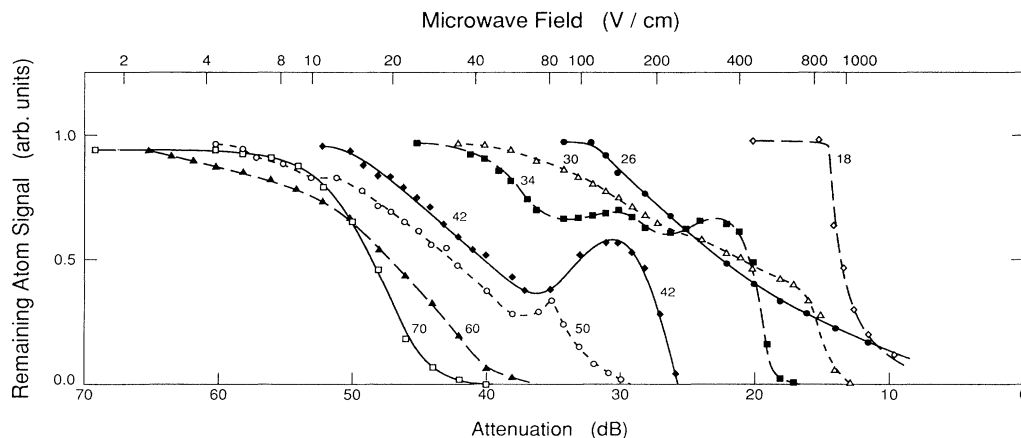


FIG. 20. Representative 4-GHz Li nd field-ionization signals obtained with $\mathbf{E}_{\text{laser}} \parallel \mathbf{E}_{\text{MW}}$ for $n = 18, 26, 30, 34, 42, 50, 60$ and 70 .

tion is not the result of many incoherent microwave cycles but a resonant multiphoton transition, and that while the requirement $E = 1/3n^5$ remains, $\omega \approx \omega_0$ does not. The measurements also show that many levels can be important.

Let us consider first the low-frequency limit, which is well represented by the Na $|m|=0$ states. At 10 MHz the Na $|m|=0$ states ionize in the same way they do with a field pulse of $\sim 1\text{-}\mu\text{s}$ rise time. For example, an atom initially in the nd state passes adiabatically through all the $E > 1/3n^5$ avoided level crossings on its way from low to high field and ionizes at point *A* of Fig. 1. As the frequency is raised to 670 MHz, we see a sharp onset of ionization at a field of $E = 1/3n^5$ and increasing ionization as the field amplitude is increased. The field of $E = 1/3n^5$ is the clear signature of the occurrence of the rate-limiting Landau-Zener transition from n to $n+1$, at point *C* of Fig. 1. Since the passage from low to high field is too slow at 10 MHz to observe anything other than an adiabatic passage, it is hardly a surprise that increasing the frequency to 670 MHz raises the probability of the n to $n+1$ transition. First, the higher frequency raises the transition probability on a single cycle, and second, there are more cycles. However, if we consider only the first $n - (n+1)$ level crossing, at $E = 1/3n^5$, calculation of the Landau-Zener transition probability on a single half cycle [6,21] shows that it is not traversed diabatically enough to yield a 1% transition probability unless E exceeds $1/3n^5$ by 30%. In other words, there is a quantitative disagreement between the result of the calculation and the observation of the sharp onset of ionization at $E = 1/3n^5$. We attribute the difference to the fact that if the field cycles add coherently the transition probability is increased. Taking into account the coherence of the transition amplitudes over many cycles, at resonance, the $n \rightarrow n+1$ transition probability T is given by

$$T_c = T_{\text{SC}} N^2 \quad (17)$$

where T_{SC} is the single-cycle transition probability and N is the number of field cycles to which the atom is exposed. We assume that T_{SC} is small, so that $T_c \ll 1$. If T_{SC} is too large Rabi oscillations occur, and Eq. (17) does not apply [22]. Incoherent addition of the transition probabilities due to N cycles yields a transition probability T_i given by

$$T_i = T_{\text{SC}} N \quad (18)$$

In practice there is likely to be a coherence time τ which limits the number of cycles which are coherent to $N_c = f\tau$, where f is the microwave frequency, so that a more realistic way of expressing T_c is

$$T_c = T_{\text{SC}} N_c^2 \quad (19)$$

If $f > 1/\tau$ the amplitudes of more than one cycle add coherently, but if $f < 1/\tau$ they do not. Thus at very low frequencies, 10 MHz, coherent effects are unimportant, and the single-cycle results apply.

As mentioned above, it is only at resonance that the transition probability is increased by the coherent addition of transition amplitudes of many field cycles. To see

the implications of the resonance requirement we show in Fig. 21(a) the static energy levels of the extreme n and $n+1$ states and in Fig. 21(b) the sidebands produced by a microwave field $E \cos \omega t$ with amplitude $E = 1/3n^5$. Due to the linear Stark shifts of the Stark states, a microwave field, $E \cos \omega t$, produces sidebands separated by ω on each of the two n states, with the sidebands extending in energy as far as the Stark shift in a dc field of magnitude E , as shown in Fig. 21. Where they overlap, the two sets of sidebands are coupled by the presence of the finite-sized ionic core, the same interaction which produces the avoided crossings of the levels in the static field [12]. For the transition to occur, a necessary condition is that the detuning Δ between the n and $n+1$ sidebands be less than the coupling between the n and $n+1$ sidebands, i.e., the Rabi frequency. If dephasing is present, due to spatial and temporal variations in the microwave field amplitude and stray fields, the energies of the levels are not constant and the resonance frequency varies spatially and temporally. In this case the Rabi frequency must be equal to the inverse of the time spent at resonance, or equivalently, to the broadening of the transition. When the microwave frequency is low, even in the two-level pic-

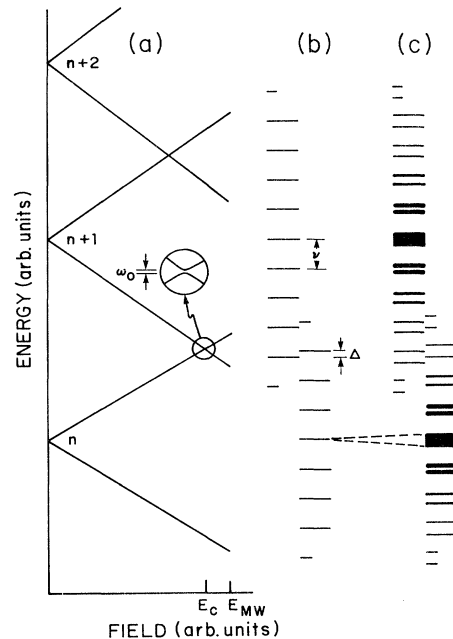


FIG. 21. (a) Static energy-level diagram showing the extreme $|m|=0$ Stark states of the n , $n+1$, and $n+2$ Stark manifolds. The extreme n and $n+1$ levels have an avoided crossing at a field of $E_c = 1/3n^5$. As shown by the inset, the magnitude is ω_0 . If a microwave field $E_{\text{MW}} \geq E_c$ is applied, atoms can make the $n \rightarrow n+1$ Landau-Zener transition at the avoided crossing, followed by successive analogous Δn transitions, culminating in ionization. (b) The spectrum of sideband states produced by a microwave field of amplitude E_{MW} and frequency ν acting on the extreme $n+1$ Stark states. The sidebands from all Stark states of the same n are degenerate modulo ω . In general there is a detuning Δ between the n and $n+1$ sidebands states. (c) The spectrum of n and $n+1$ sideband states upon the application of a small static electric field which removes the degeneracy of the sideband states originating from different Stark states.

ture of Figs. 21(a) and 21(b), only small changes in the level spacings, due to, for example, small variations in the field intensity, can bring the levels into resonance. In fact, Figs. 21(a) and 21(b) are oversimplifications since the $n \rightarrow n+1$ transitions can occur between any pair of n and $n+1$ Stark levels which have adequate coupling. To a first approximation the k th sidebands of different Stark levels of the same n are degenerate. However, their degeneracy is lifted by their differing amounts of core interaction [3], and also their different second-order Stark shifts [23]. The core interaction shifts the energies of the Stark states [3] by an amount $\sim \delta_m/n^4$, and there is a dispersion in the shifts around this value. Since the s quantum defects contribute, in principle, equally to all the Stark states, the maximum dispersion is due to the p states which in Na have a quantum defect (mod1) of -0.15 . The order of magnitude of the energy splitting between adjacent Na Stark states of $|m|=0$ or 1 is, therefore, $\sim \delta_p/n^5$, which is ~ 300 MHz at $n=20$. At $n=20$ the difference in the second-order Stark shifts between adjacent extreme Stark states of $|m| \ll n$ in a field $E=1/3n^5$ are $\sim 1/12n^5$, or ~ 20 MHz. These splittings ensure that for microwave frequencies < 1 GHz a resonance between nearly extreme n and $n+1$ Stark states is virtually certain to occur at $E \approx 1/3n^5$.

While the resonance condition is easily met at low frequencies, broadening of the levels implies that coherence is maintained over a smaller number of field cycles than at higher frequencies. In practical cases the single-cycle Landau-Zener model and the resonant multiphoton picture converge as the frequency is reduced.

At the other extreme, $\omega \gg \omega_0$, both the single-cycle Landau-Zener model and the resonant multiphoton model predict negligible ionization at $E=1/3n^5$. The reason for negligible ionization in the multiphoton picture can be inferred from Fig. 21(b). When $\omega \gg \omega_0$ the applied frequency is very large compared to the coupling between the levels. Thus the Rabi frequency is much smaller than spacing of the sidebands. In the unlikely event of no broadening only transitions with very small detunings will occur. In the presence of broadening there is simply not enough coupling to drive the transitions.

At first glance it is not apparent that at high frequency it is possible to discriminate between the two models. In fact from the zero-field data it is not possible to do so. However, the fact that adding a small static field leads to ionization by a microwave field of $E \approx 1/3n^5$, instead of $E=1/9n^4$, allows us to discriminate between the two models. Adding a small static field has negligible effect in a single-cycle Landau-Zener picture. In contrast it has a substantial effect on resonant multiphoton transitions when all the levels of the Stark manifold are taken into account. The effect, termed quasicontinuum production, is easily understood in a sideband picture. In the sideband picture of Fig. 21(b) the effect of a small static field E_s is to shift the sidebands of the extreme blue n and red $n+1$ Stark states up and down in frequency by $\frac{3}{2}n^2E_s$, respectively. If these two levels were the only two possible levels, we might expect to see sharp increases in the transition probability at the static fields which bring the n and $n+1$ levels into resonances, as has been observed by

Stoneman, Thomson, and Gallagher [12], but no such sharp resonances are observed. Apparently more than just the extreme Stark states participate in the $n \rightarrow n+1$ transition.

In the sideband picture of Fig. 21(b) all the n Stark states have sideband energies which are nearly degenerate. Applying the reasoning used for Na to Li, which has an np quantum defect of 0.05, the splittings of adjacent extreme Li $|m|=0$ or 1 Stark states are ~ 100 MHz, and the second-order Stark splittings are ~ 20 MHz, both of which are negligible compared to a microwave frequency of 10 GHz. For our purposes, therefore, sidebands generated by a microwave field are degenerate for different Stark states. Applying a static field as well lifts the degeneracy of the k th sidebands of different Stark states, and what are shown as single sideband energies in Fig. 21 becomes groups of levels split by the static Stark shifts of those states which have sidebands at that energy. Only the extreme positive and negative Stark states have non-negligible amplitudes in the sidebands farthest removed from the zero-field energies; thus these sidebands are only split into two levels $3n^2E_s$ apart. Near the zero-field energy, nearly all the Stark states have appreciable sideband amplitudes and at each sideband energy there are n levels spanning an energy range $3n^2E_s$. If

$$3n^2E_s = \omega, \quad (20)$$

at the zero-field energies of the n and $n+1$ states there is a uniform distribution of sideband states ω/n apart in energy. The small energy spacing greatly enhances the probability of the microwave frequency's matching the multiphoton resonance frequency. We have previously tested the validity of these notions by measuring the static fields required to produce ionization of the Li nd states by 8- and 15-GHz fields at $E \approx 1/3n^5$ instead of $E=1/9n^4$. For a fixed microwave field in excess of $1/3n^5$ microwave ionization increases dramatically, often from $\sim 10\%$ to $\sim 90\%$, as the static field is raised from zero to a small (~ 1 V/cm) field after which there is no further increase. The static field E_s at which half the increase in the microwave ionization occurs is straightforward to measure, and experimentally this field, at both 8 and 15 GHz, is $\omega/6n^2$. Since the full enhancement of the ionization occurs at about twice this field, i.e., at $E_s = \omega/3n^2$, these observations correspond to Eq. (20). The striking effect of small fields is strong evidence that the rate limiting $n \rightarrow n+1$ transitions are resonant multiphoton transitions between many levels.

In the very-high-frequency limit where the microwave frequency ω becomes a small multiple of the Δn energy spacing, $1/n^3$, the microwave field no longer leads to ionization at $1/9n^4$, but at a lower field [11]. This is shown in Figs. 14, 17, and 19 for the high- n thresholds which fall below the $1/9n^4$ field dependence. For these states the motion of the Rydberg electron, and ionization, has been referred to as chaotic [17–19]. An alternative picture, which relates to the quantum-mechanical one developed here, views the ionization process as a sequence of multiphoton Δn transitions in which the rate-limiting step is the $n \rightarrow n+1$ transition [13].

V. CONCLUSION

In summary, these measurements show an interesting evolution from 10 MHz to 15 GHz. In this frequency regime a model based on Landau-Zener transition between the extreme n and $n + 1$ Stark states in a single microwave cycle is inadequate. These experiments indicate that in this regime both multiple-cycle effects and the presence of many level crossings at $E > 1/3n^5$ are impor-

tant, as indicated by the theoretical work of Christiansen-Dalsgaard [13].

ACKNOWLEDGMENTS

This work has been supported by the U.S. Air Force Office of Scientific Research under Grant No. AFOSR-90-0036. It is a pleasure to acknowledge stimulating discussions with B. Christiansen-Dalsgaard.

*Permanent address: Laboratoire Aimé Cotton, Centre National de la Recherche Scientifique II, Bâtiment 505, Campus d'Orsay 91405 Orsay CEDEX, France.

†Permanent address: United States Naval Research Laboratory, Laser Physics Branch, Code 6540, 4555 Overlook Avenue S.W., Washington, DC 20375.

- [1] M. G. Littman, M. M. Kash, and D. Kleppner, *Phys. Rev. Lett.* **41**, 103 (1978).
- [2] W. Sandner, K. A. Safinya, and T. F. Gallagher, *Phys. Rev. A* **33**, 1008 (1986).
- [3] I. V. Komarov, T. P. Grozdanov, and R. K. Janev, *J. Phys.* **13**, L573 (1980).
- [4] T. F. Gallagher, L. M. Humphrey, W. E. Cooke, S. A. Edelslein, and R. M. Hill, *Phys. Rev. A* **16**, 1098 (1977).
- [5] T. H. Jeys, G. W. Foltz, K. A. Smith, E. J. Beiting, F. G. Kellert, F. B. Dunning, and R. F. Stebbings, *Phys. Rev. Lett.* **44**, 390 (1980).
- [6] P. Pillet, H. B. van Linden van den Heuvell, W. W. Smith, R. Kachru, N. H. Tran, and T. F. Gallagher, *Phys. Rev. A* **30**, 280 (1984).
- [7] P. Pillet, W. W. Smith, R. Kachru, N. H. Tran, and T. F. Gallagher, *Phys. Rev. Lett.* **50**, 1042 (1983).
- [8] D. R. Mariani, W. van de Water, P. M. Koch, and T. Bergeman, *Phys. Rev. Lett.* **50**, 1261 (1983).
- [9] H. B. van Linden van den Heuvell and T. F. Gallagher, *Phys. Rev. A* **32**, 1495 (1985).
- [10] C. E. Moore, *Atomic Energy Levels*, Natl. Bur. Stand. (U.S.) Circular No. 467 (U.S. GPO, Washington, DC, 1949).
- [11] T. F. Gallagher, C. R. Mahon, P. Pillet, Panming Fu, and J. B. Newman, *Phys. Rev. A* **39**, 4545 (1989).
- [12] R. C. Stoneman, D. S. Thomson, and T. F. Gallagher, *Phys. Rev. A* **37**, 1527 (1988).
- [13] B. L. Christiansen-Dalsgaard (unpublished).
- [14] J. P. Montgomery, *IEEE Trans. Microwave Theory Tech.* **MTT-19**, 547 (1971).
- [15] A. J. Hatch and H. B. Williams, *Phys. Rev.* **112**, 681 (1958).
- [16] R. G. Rolfes, D. B. Smith, and K. B. MacAdam, *J. Phys.* **16**, L535 (1983).
- [17] K. A. H. van Leeuwen, G. V. Oppen, S. Renwick, J. B. Bowlin, P. M. Koch, R. V. Jensen, O. Rath, D. Richards, and J. G. Leopold, *Phys. Rev. Lett.* **55**, 2231 (1985).
- [18] I. C. Percival, *J. Phys. B* **6**, L229 (1973).
- [19] R. V. Jensen, *Phys. Rev. A* **30**, 386 (1984).
- [20] P. Pillet, C. R. Mahon, and T. F. Gallagher, *Phys. Rev. Lett.* **60**, 21 (1988).
- [21] J. R. Rubbmark, M. M. Kash, M. G. Littman, and D. Kleppner, *Phys. Rev. A* **23**, 3107 (1981).
- [22] N. F. Ramsey, *Molecular Beams* (Oxford University Press, London, 1956).
- [23] H. A. Bethe and E. A. Salpeter, *Quantum Mechanics of One and Two Electron Atoms* (Plenum, New York, 1977).

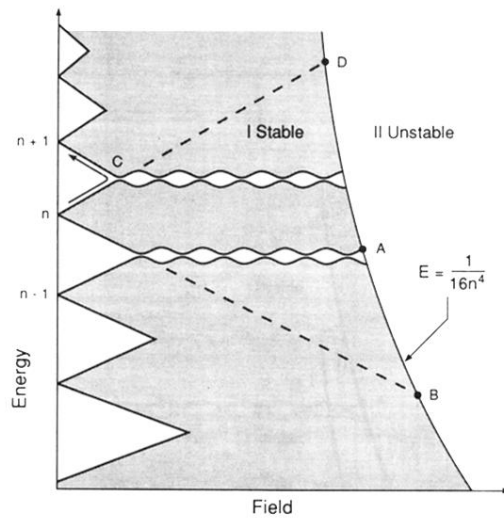


FIG. 1. Schematic drawing of the $n - 1$, n , and $n + 1$ Stark manifolds. Where the manifolds intersect the states have avoided crossings ω_0 . For ionizing fields with low slew rates the passage from low to high field is adiabatic and the red Stark state of n ionizes at the classical ionization limit at the field $1/16(n - 1/2)^4$, point A . For ionizing fields with high slew rates the passage is diabatic and the red Stark state ionizes at the classical limit at the field $1/9n^4$, point B . The blue Stark state may ionize at the field $1/21n^4$ (point D) only by coupling to a rapidly ionizing red Stark state of high n . In a microwave field $E \geq 1/3n^5$ the atom ionizes via a sequence of Δn Landau-Zener transitions with the rate-limiting step being the $n \rightarrow n + 1$ transition, point C .